2–10 μm Mid-Infrared Fiber-Based Supercontinuum Laser Source: Experiment and Simulation

Sebastien Venck, François St-Hilaire, L Brilland, Amar Nath Ghosh, Radwan Chahal, Céline Caillaud, Marcello Meneghetti, J Troles, Franck Joulain, Solenn Cozic, et al.

2-10 μm Mid-Infrared All-Fiber Supercontinuum Laser Source: Experiment and Simulation

Sébastien Venck[1], François St-Hilaire[2,6], Laurent Brilland[1], Amar N. Ghosh[2], Radwan Chahal[1], Céline Caillaud[1], Marcello Meneghetti[3], Johann Troles[3], Franck Joulain[4], Solenn Cozic[4], Samuel Poulain[4], Guillaume Huss[5], Martin Rochette[6], John Dudley[2], and Thibaut Sylvestre*[2]

[1]SelenOptics, Campus de Beaulieu, Rennes, France
[2]Institut FEMTO-ST, CNRS UMR 6174, Université Bourgogne Franche-Comté, Besançon, France
[3]Université de Rennes, CNRS, ISCR-UMR 6226, Rennes, France
[4]Le Verre Fluoré, Campus Kerlann, Bruz, France
[5]LEUKOS, 37 rue Henri Giffard, Limoges, France
[6]Department of Electrical and Computer Engineering, McGill University, Montréal, Québec, Canada

December 20, 2019

Abstract

Mid-infrared supercontinuum (SC) sources in the 2 to 20 μm molecular fingerprint region are in high demand for a wide range of applications including optical coherence tomography, remote sensing, molecular spectroscopy, and hyperspectral imaging. In this work, we investigate mid-IR SC generation in a cascaded silica-ZBLAN-chalcogenide fiber system directly pumped with a commercially-available 460-ps pulsed fiber laser operating in the telecommunications window at 1.55 μm. This all-fiber system is shown to generate a flat broadband mid-IR SC covering the entire range from 2 to 10 μm with several tens of mW of output power. This technique paves the way for cheaper, practical, and robust broadband SC sources in the mid-IR without the requirement of mid-infrared pump sources or Thulium-doped fiber amplifiers. We also describe a fully-realistic numerical model used to simulate the nonlinear pulse propagation through the cascaded fiber system and we use our numerical results to discuss the physical processes underlying the spectral broadening in the cascaded system. We conclude with recommendations to optimize the current cascaded systems based on our simulation results.

*corresponding author: thibaut.sylvestre@univ-fcomte.fr

1 Introduction

Fiber-based supercontinuum (SC) sources have become enormously useful in the last decade in wide range of industrial and scientific applications [1, 2]. New uses are constantly emerging due to their unique properties that combine high brightness, multi-octave frequency bandwidth, fiber delivery and single-mode output. Applications include optical coherence tomography (OCT), material processing, chemical sensing, gas monitoring, broadband imaging, absorption spectroscopy. Currently, there is a significant research effort focused on extending the wavelength coverage towards the mid-Infrared (Mid-IR) in the 2 to 20 μm molecular fingerprint region [3–18]. Various soft glasses based on chalcogenide (As_2S_3, As_2Se_3, GeAsSe) [3, 8], tellurite (TeO_2) [19], telluride (GeTe, GeAsTeSe) [20, 21], heavy-metal oxide (PbO-Bi_2O_3-Ga_2O_3-SiO_2-CdO) [10] and ZBLAN (ZrF_4 –BaF_2 –LaF_3 –AlF_3 –NaF) [23, 24, 26], have been used for drawing highly nonlinear infrared fibers, and experiments have shown efficient mid-IR SC generation up to 14 μm in chalcogenide optical fibers and up to 16 μm in telluride fibers [3, 21]. However, most of these mid-IR SC sources have been demonstrated using bulky mid-IR pump sources such as optical parametric oscillators (OPO) and amplifiers (OPA). Mid-IR fiber lasers and cascaded fiber systems have recently emerged as very attractive and promising solutions for practical and commercial applications [25–33, 35]. These all-fiber systems indeed open routes to practical, table-top and robust mid-IR supercontinuum lasers with high spectral power density. Of particular interest are cascaded fiber systems as they are pumped by standard pulsed fiber lasers at telecommunication wavelength. In cascaded SC generation, an initial pulsed fiber laser at 1550 nm is progressively red-shifted in a cascade of silica and soft-glass fibers, enabling a stepwise extension towards the Mid-IR. From a fundamental point of view, the overall objective is to strongly enhance the soliton self-frequency shift (SSFS) using dispersion-tailored highly nonlinear fiber segments to push forward the SC generation far in the mid-IR [31].

Among the most advanced all-fiber systems, Martinez et al. recently demonstrated a mid-IR SC from 2 to 11 μm with 417 mW on-time average power by concatenating solid-core ZBLAN, arsenic sulfide, and arsenic selenide fibers, pumped by a master oscillator power amplifier and three thulium-doped fiber amplifier stages [29, 30]. Hudson et al. combined a 2.9 μm ultrafast fiber laser based on holmium with an environmentally stable, polymer-protected chalcogenide fiber taper. By launching femtosecond, 4.2 kW peak power pulses into the As_2Se_3/As_2S_3 tapered fiber, they demonstrated a SC spectrum spanning from 1.8 to 9.5 μm with an average power of more than 30 mW [27]. C.R. Petersen et al. also demonstrated in 2016 Mid-IR SC generation beyond 7 μm using a silica-fluoride-chalcogenide fiber cascade pumped by a 1.55 μm seed laser and a thulium-doped fiber amplifier. By pumping a commercial $Ge_{10}As_{22}Se_{68}$-glass photonic crystal fiber with 135 mW of the pump continuum from 3.5- 4.4 μm, they obtained a continuum up to 7.2 μm with a total output power of 54.5 mW, and 3.7 mW above 4.5 μm [33]. Commercially available mid-IR SC source with an extended bandwidth up to 10 μm and with 50 mW output power is now on sale at Norblis [34].

In this paper, we demonstrate all mid-IR all-fiber SC generation from to 2 to 10 μm in a cascaded silica-ZBLAN-As_2Se_3 chalcogenide fiber system directly pumped with a commercially-available 500-ps pulsed fiber laser at 1.55 μm and without any fiber amplifier stage. We provide the details of the experimental cascaded fiber system and discuss the parameters as dispersion and nonlinear coefficients used for optimal spectral broadening. We further report a fully-realistic numerical model based on cascaded generalized nonlinear Schrödinger equations with an adaptive step size method. The model includes all the linear and nonlinear responses of the fibers, the infrared filtering function, and the effective mode area variation across the full SC spectrum. We then use our numerical results to discuss the physical processes underlying the spectral broadening in the cascaded system as modulation instability (MI), soliton fission and dispersive wave generation [1,2,36,37]. We conclude with recommendations to optimize the current cascaded systems based on our simulation results.

2 Experimental Setup and Results

A diagram of the experimental setup for cascaded mid-IR SC generation is shown in Figure 1(a). It consists of a concatenation of three different optical fibers including a short 20 cm-long single-mode silica fiber (SMF-28), a 25m-long ZBLAN fiber, and a 9-m long chalcogenide-glass photonic crystal fiber, all commercially available. Detailed specifications for each fiber segment are given in the next section including all parameters used in numerical simulations. This cascaded fiber arrangement was directly pumped by a 1550.6 nm Erbium-doped fiber laser delivering 460 ps pulse train at 90 kHz repetition rate and with an average output power of 750 mW. For a pulse energy of 8.33 μJ and a pulse duration around 460 ps, the corresponding pulse peak power is around 18 kW. Light coupling between each fiber was achieved using high-numerical aperture aspheric lenses matching the fiber numerical apertures and their effective mode areas. A key element in the cascaded fiber system is a mid-IR long pass filter (LPF) placed in between the ZBLAN and the chalcogenide fibers. This filter that filters out all the wavelengths below 1.9 μm. This prevents from two-photon absorption (TPA) and optical damage in the chalcogenide fiber, enabling a better long-term stability of the mid-IR SC source. As a long-pass filter, we used a Germanium (Ge) Ar-coated broadband window (Thorlabs WG91050) in between two aspheric lenses. The generated SC spectra have been recorded using a mid-IR optical spectrometer including a monochromator (ORIEL 7240) and a highly sensitive Hg-Cd-Te detector. The chalcogenide fiber output end was further connectorized using an FC/PC connector for pratical applications.

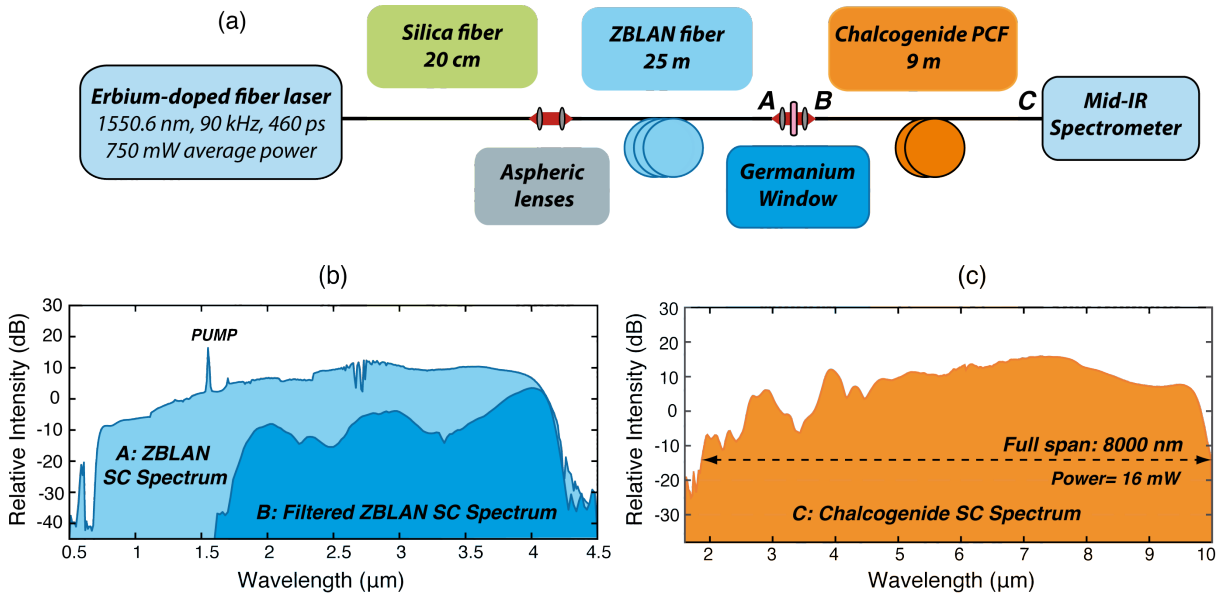

Figure 1: (a) Experimental setup for mid-infrared SC generation in a cascaded silica-ZBLAN-chalcogenide optical fiber system. (b) Experimental SC spectra at the ZBLAN fiber output (blue) and after the long-pass filter (red). (c) Experimental SC spectrum at the chalcogenide fiber output (yellow).

We provide experimental data for the spectra measured at three key points in the cascaded fiber setup (A,B,C). The first spectrum, shown in Figure 1(b) (light blue), was measured directly at the output of the ZBLAN fiber at point A, before the long-pass infrared filter. The supercontinuum spans from 0.7 μm up to 4.1 μm. The second spectrum, also shown in figure 1(b) (dark blue), was measured after the filter at point B. This is the filtered IR spectrum injected into the chalcogenide fiber. The final SC spectrum at the output of the chalcogenide fiber is shown in figure 1(c) in yellow. As can be seen, the full SC spans from 2

μm up to 9.8 μm with a relatively smooth and flat bandwidth. The measured spectrum however shows a decrease in spectral intensity for shorter wavelengths and significant modulations in intensity (especially from 2 to 4 μm). Our simulations will show that those are not entirely a result of SC dynamics, but presumably artefacts from the wavelength sensitivity of the spectrometers used for measurement. The measured average power at the output is 16 mW, which corresponds to roughly 2% of the pump's average power (750 mW). Significant losses occur in the cascaded system, mainly from the free-space optics between the ZBLAN fiber and the chalcogenide fiber, including Fresnel reflections and coupling losses due to mode field diameter mismatch, aspheric lenses, cleaving imperfections, and optical misalignment. Despite this low conversion efficiency, the brightness of this source of a few microwatt per nanometer is sufficient for practical applications.

3 Numerical Method

To simulate nonlinear pulse propagation in the cascaded fiber system, we used the generalized nonlinear Schrödinger equation (GNLSE) and solved the propagation equation numerically with the split-step Fourier method (SSFM) [2, 37] combined with an adaptive step size [44]. The GNLSE can be written in the following form:

$$\frac{\partial A(z,T)}{\partial z} = -\frac{\alpha}{2}A + \mathrm{i}\sum_{k=2}^{\infty}\frac{\mathrm{i}^k\beta_k}{k!}\frac{\partial^k}{\partial T^k}A + \mathrm{i}\gamma\left(1+\mathrm{i}\tau_0\frac{\partial}{\partial T}\right)\left[A\cdot R(T)\circledast|A|^2\right] \tag{1}$$

This equation models the evolution of the complex pulse envelope $A(z,T)$ as it propagates inside an optical fiber in a frame of reference moving with the group velocity of the pulse: $T = t - \beta_1 z$. The first term on the right models optical losses with the linear loss coefficient α. The second term models dispersion with a Taylor expansion of the propagation constant $\beta(\omega)$, where $\beta_k = \frac{\partial^k \beta(\omega)}{\partial \omega^k}$. The third term models Kerr nonlinearity, including the Raman response of the material and a first-order correction for the frequency dependence of the nonlinear parameter γ, $\gamma(\omega) = \frac{\omega n_2(\omega)}{cA_{\mathrm{eff}}(\omega)}$. The first-order correction is referred to as the *shock* term and is characterized by a time-scale τ_0, which can include the frequency-dependence of A_{eff}, n_2, and n_{eff} (see [43] for more details).

$$\tau_0 = \frac{1}{\omega_0} - \left[\frac{1}{n_{\mathrm{eff}}(\omega)}\frac{\mathrm{d}n_{\mathrm{eff}}}{\mathrm{d}\omega}\right]_{\omega_0} - \left[\frac{1}{A_{\mathrm{eff}}(\omega)}\frac{\mathrm{d}A_{\mathrm{eff}}}{\mathrm{d}\omega}\right]_{\omega_0} + \left[\frac{1}{n_2(\omega)}\frac{\mathrm{d}n_2}{\mathrm{d}\omega}\right]_{\omega_0} \tag{2}$$

The nonlinear response of the fiber is modeled with a convolution (denoted by $\circledast$) of the nonlinear response function $R(T)$ and the pulse power profile $|A(z,T)|^2$. $R(T)$ is commonly divided into an instantaneous electronic response (Kerr) and a delayed molecular response (Raman), and reads as $R(T) = (1-f_R)\delta(T) + f_R h_R(T)$, where f_R is the fractional contribution of the delayed Raman response, $\delta(T)$ is the Dirac delta function that models the instantaneous Kerr response, and $h_R(T)$ is the delayed Raman response function. $R(T)$ is normalized such that $\int_{-\infty}^{\infty} R(T)\mathrm{d}T = 1$. The Raman response function $h_R(T)$ is modeled using two characteristic times related to phonon dynamics in the material, τ_1 and τ_2 (see Ref [37] for more details):

$$h_R(T) = (\tau_2^{-2} + \tau_2^{-2})\tau_1 \exp(-T/\tau_2)\sin(T/\tau_1) \tag{3}$$

We will use Eq. (3) for both the silica and chalcogenide fibers (See Table 1 for parameters). However, as the ZBLAN fiber has a dual-peak Raman gain spectrum, we will another model based on Eq. 5. A crucial step in modeling nonlinear pulse propagation in a cascaded fiber system is defining the longitudinal step size h. To accurately model the effects of nonlinearity and dispersion, h must be much smaller than both the dispersion length and the nonlinear length, defined as, $L_{\mathrm{NL}} = \frac{1}{\gamma P_0}$ and $L_{\mathrm{D}} = \frac{T_0^2}{|\beta_2|}$, respectively,

where P_0 is the peak power, and T_0 is the $1/e$ pulse width. These two conditions must hold throughout the propagation length. Pumping with a quasi-continuous-wave laser (i.e. 460 ps pulses) leads to the break-up of the initial pulse via modulation instability (MI) into a huge number of ultrashort soliton-like pulses with variable peak powers P_0 and durations T_0. The choice of h is therefore not as straightforward in this case. Our simulations show that the nonlinear length L_{NL} is a much more limiting factor than the dispersion length L_{D} for the step size h because of the high peak power reached within the soliton train. When the soliton train starts propagating, the maximal peak power varies significantly along the propagation distance z because of randomly occurring soliton collisions. This means that the condition $h << L_{\mathrm{NL}}$ can change drastically along z. To account for this, we used an adaptive step size method for our SSFM algorithms: the nonlinear phase-rotation method (see [44] for more details). This method consists of limiting the nonlinear phase-shift $\phi_{\mathrm{NL}} = \gamma P_0 h$ to a sufficiently small value at each iteration, i.e. the step size h is adapted at each iteration to optimize computing time and accuracy. For a train of soliton pulses, the maximal phase-shift is calculated from the maximal soliton peak power P_0^{max}. Every iteration i, the step size $h(i)$ is determined by $h(i) = \frac{\phi_{\mathrm{NL}}^{max}}{\gamma_0 P_0^{max}(i)}$. For our simulations, we found that a maximal nonlinear phase-shift of $\phi_{\mathrm{NL}}^{max} = 1/50$ rad is enough for convergence and allows for reasonable computing times.

3.1 Cascaded fiber system

This section provides all linear and nonlinear parameters of the cascaded fiber system used in numerical simulations. The first fiber segment consists of a short length of 20 cm of standard single-mode silica fiber (SMF-28). Although this fiber plays a little role in SC broadening, it serves as a nonlinear modulation instability stage that triggers the soliton dynamics in both the ZBLAN and chalcogenide fibers. The nonlinear parameters for fused silica fiber are taken from [37] and are shown in Table 1.

Table 1: Nonlinear parameters for the cascaded fiber system

Fiber	L (cm)	n_2 (cm^2/W)	$\mathrm{A_{eff}}$ ($\mu\mathrm{m}^2$)	γ ($\mathrm{W}^{-1}\mathrm{km}^{-1}$)	f_R	τ_1 (fs)	τ_2 (fs)
SMF-28	20	$2.4{\cdot}10^{-16}$	85	1.3	0.18	12.2	32
ZBLAN	2500	$2.1{\cdot}10^{-16}$	43	2	0.2	Eq. 5	Eq. 5
Chalcogenide	900	$1.1{\cdot}10^{-13}$	62	720	0.1	23.2	195

The wavelength dependence of $\mathrm{A_{eff}}$ and n_2 is negligible over the spectral bandwidth along this first fiber segment. The dispersion characteristics of SMF-28 are modeled using a Taylor series expansion. The following values are used: $\beta_2 = -21.4 \cdot 10^{-27}$ s^2/m, $\beta_3 = 0.12 \cdot 10^{-39}$ s^3/m (from [37]). The 1550 nm pump is in the anomalous dispersion regime. Optical losses were neglected for this fiber segment given the short length (20 cm) and low absorption of silica fibers at 1550 nm (0.2 dB/km).

The second fiber consists of a length of 25 m of a commercially available step-index fluoride (ZBLAN) fiber from Le Verre Fluoré [40]. The core and cladding diameters are 8.5 μm and 125 μm, respectively. The refractive index of core and cladding are plotted in Figure 2(a) and the dispersion curve is shown in Fig. 2(b) in blue. Experimental data of dispersion from 1.2 to 2.2 μm are provided in red dots. To obtain the dispersion of the fiber over the full bandwidth, we solved the characteristic equation for a step-index fiber with the wavelength-dependent core and cladding indices shown in figure 2(a). Results show that the zero dispersion wavelength (ZDW) is 1525 nm. Therefore the 1550 nm pump wave is in the slightly anomalous dispersion regime.

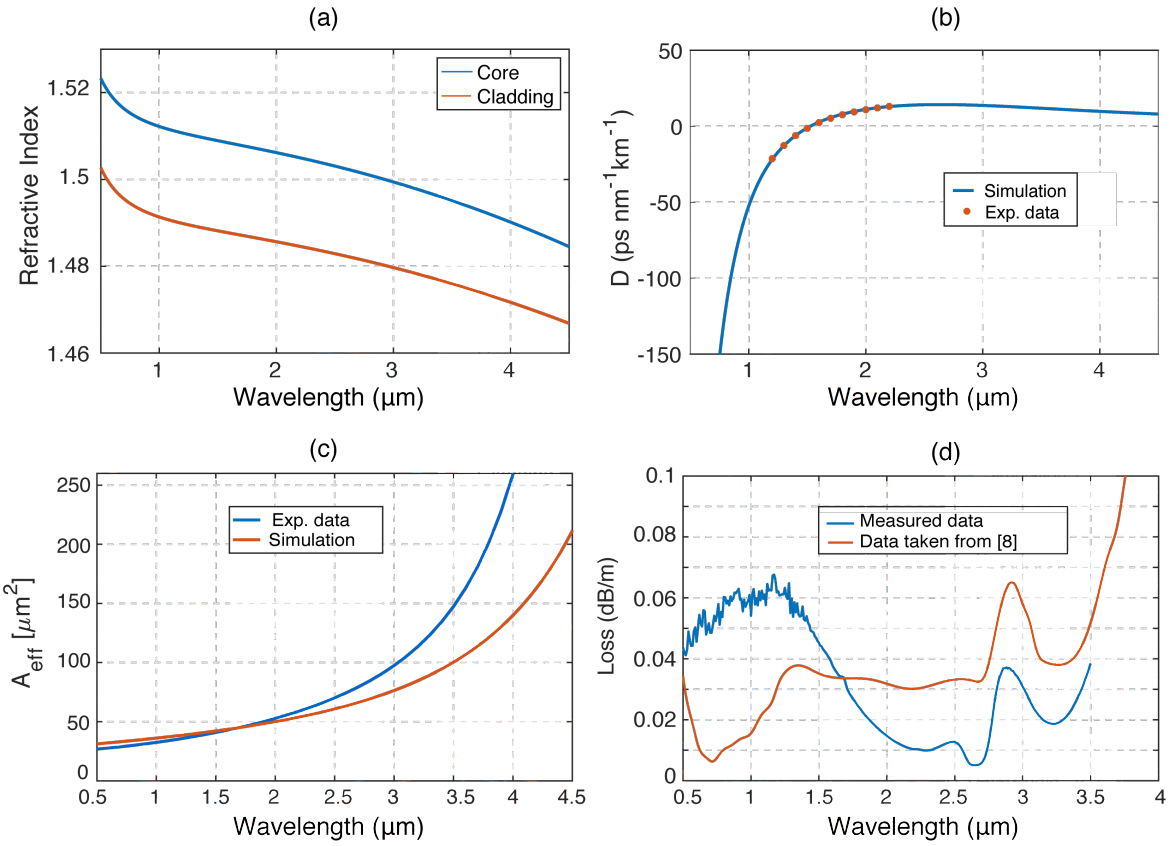

Figure 2: ZBLAN step-index optical fiber specifications: (a) Core (blue) and cladding (Red) refractive indices versus wavelength. (b) Computed dispersion (blue curve) and experimental data (Red dots). (c) Simulated (red) and experimental (blue) effective mode area. (d) Loss spectrum: blue: Measured data, red: data from [41]

The strong effective mode area variation from 0.5 to 5 μm was also considered. We calculated A_{eff} over the same bandwidth by solving the characteristic equation for a step-index fiber with the wavelength-dependent core and cladding indices. The results are compared with the experimental data in Fig. 2(c). Our simulated results were used instead of the measured data because it provided a better fit with the experimental SC when the wavelength dependence of A_{eff} was included.

Figure 2(d) shows the optical losses of the ZBLAN fiber. The measurements are shown in blue, and the data used in the simulations (taken from [41]) is shown in orange. The data from [41] was used in our simulations to better model the limit of the transmission window in the infrared, which ends between 4 and 4.5 μm. As we will show in our results, the transmission window limit of the ZBLAN fiber is the only feature of the loss curve that has a significant impact on spectral nonlinear dynamics. The small discrepancies with the measured loss curve should not affect the overall SC mechanisms.

The nonlinear parameters for the ZBLAN fiber are listed in Table 1. The wavelength dependence of the nonlinear index is neglected. The Raman response function h_R was obtained with the model developed in Ref. [24], where the measured Raman gain spectrum $g_R(\Omega)$ is approximated by a sum of two Gaussian functions, and the response function is extracted from the imaginary part of the Fourier transform as

$$h_R(T > 0) = C \cdot \int_0^\infty g_R(\Omega) \sin(\Omega T) \mathrm{d}\Omega \tag{4}$$

where C is a normalization constant chosen such that $\int_{-\infty}^{\infty} h_R(T)\mathrm{d}T = 1$. The following equation was

used in our simulations to model $g_R(\Omega)$:

$$g_R(\Omega) = a_1 \exp\left(\frac{(\Omega/(2\pi) - \nu_1)^2}{2\omega_1^2}\right) + a_2 \exp\left(\frac{(\Omega/(2\pi) - \nu_2)^2}{2\omega_2^2}\right) \tag{5}$$

with $a_1 = 0.54 \cdot 10^{-11}$cm/W, $a_2 = 0.25 \cdot 10^{-11}$cm/W, $\nu_1 = 17.4$ THz, $\nu_2 = 12.4$ THz, $\omega_1 = 0.68$ THz, $\omega_2 = 3.5$ THz [24]. $g_R(\Omega)$ is plotted in Figure 3. Here, the anti-Stokes absorption is neglected in the frequency-domain Raman response.

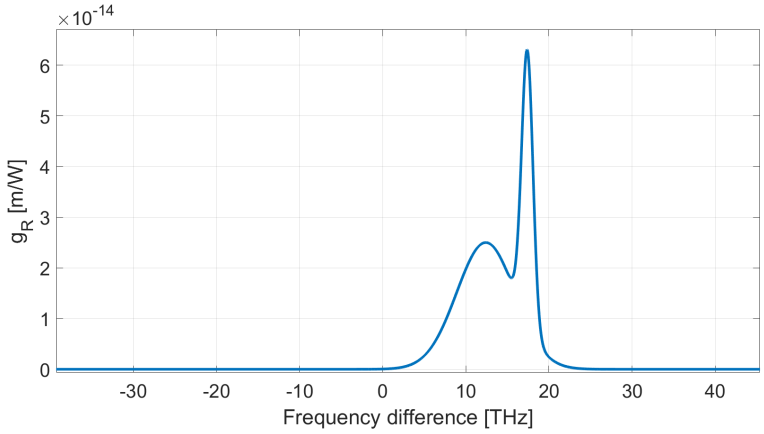

Figure 3: Raman gain numerical model for the ZBLAN fiber.

The third fiber sample is a chalcogenide-glass solid-core microstructured optical fiber. It was fabricated from $As_{38}Se_{62}$ glass using the stack and draw method [45]. It has a core diameter of 11.2 μm, a pitch of 7.11 μm, and an air-hole diameter of 3.23 μm. Figure 4 shows a cross section of the microstructure with dimensions for the air hole structure (a) as well as the refractive index of $As_{38}Se_{62}$ glass (b). The following Sellmeier model was used, $n^2 = A_0 + \frac{A_1\lambda^2}{\lambda^2 - a_1^2} + + \frac{A_2\lambda^2}{\lambda^2 - a_2^2}$, with $A_0 = 3.7464$, $A_1 = 3.9057$, $A_2 = 0.9466$, $a_1 = 0.4073$ μm, and $a_2 = 40.082$ μm. These values were chosen to obtain the best fit with the refractive index measured data shown in Fig.4(a).

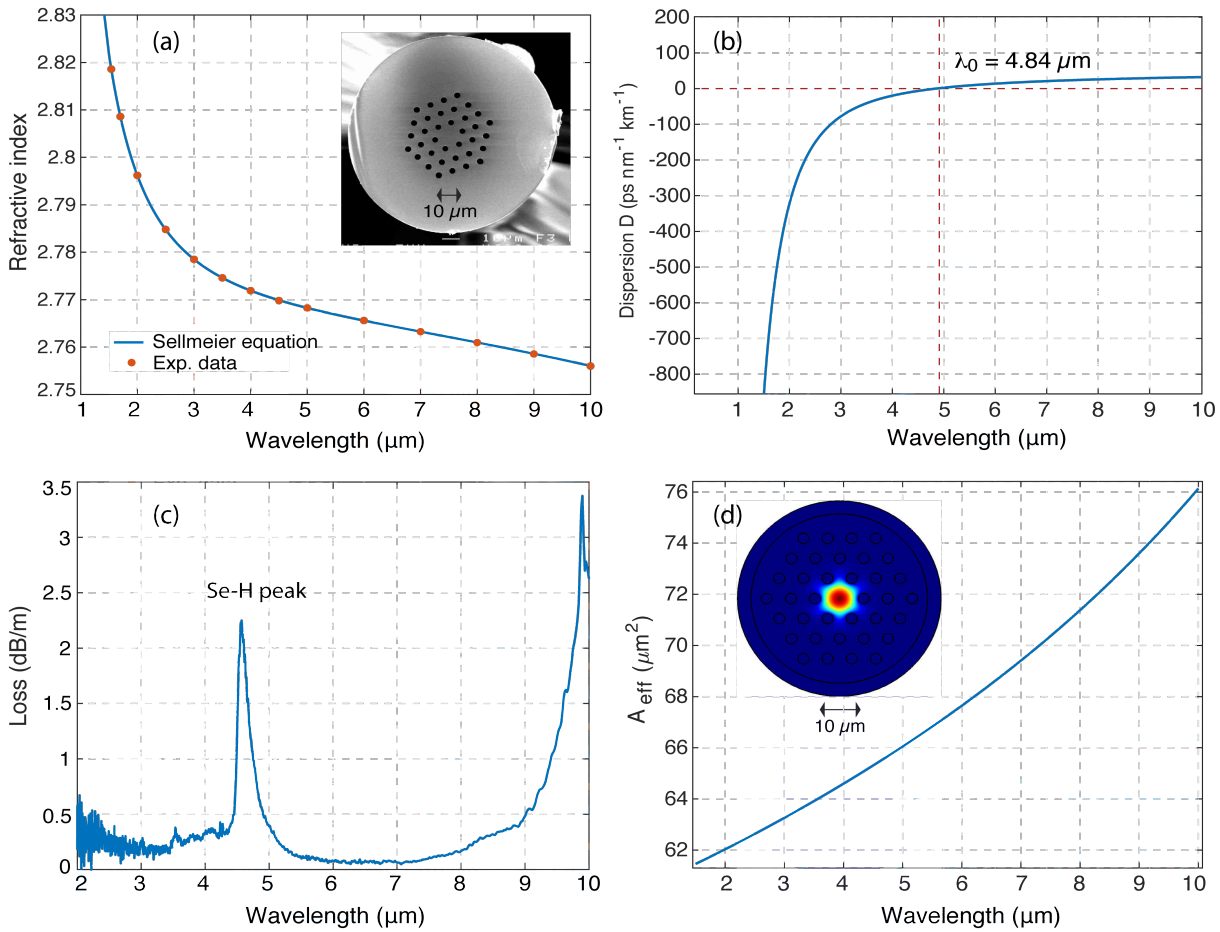

Figure 4: (a) Refractive index of $As_{38}Se_{62}$ glass calculated with the Sellmeier model. Inset shows the cross-section image of the microstructured chalcogenide fiber. (b) Computed dispersion curve for the microstructured chalcogenide fiber with a zero dispersion wavelength near 5 μm. (c) Absorption loss of the chalcogenide-based microstructured fiber. (d) Computed effective mode area. Inset shows the fundamental optical HE_{11} mode.

The dispersion curve for the fundamental mode was calculated by the finite-element method using the COMSOL software. The result is shown in Fig. 4(a). The zero-dispersion wavelength is 4.84 μm. The calculated effective mode area is shown in figure 4(d). Optical losses for the chalcogenide fiber are shown in figure 4(c). The transmission window ends near 10 μm, and there is an absorption peak around 4.56 μm due to the presence of Se-H chemical bounds in the glass. The nonlinear parameters considered for this $As_{38}Se_{62}$ glass fiber are summarized in table 1. The nonlinear index n_2 is taken from [2] and is considered constant across the 2-10 μm bandwidth. The Raman response is modelled with equation 3 and the Raman parameters are taken from [42]. This gives Raman gain peak centered around 6.9 THz with a linewidth of about 3.2 THz.

3.2 Infrared Optical Filter

The short-wavelength filtering of the ZBLAN fiber output is achieved experimentally with a combination of a germanium window (THORLABS WG91050-C9) and lenses with Ar anti-reflective coatings. This filtering window aims to cut all the energy below 1.9 μm in the ZBLAN fiber output spectrum to prevent two-photon absorption and optical damage in the chalcogenide optical fiber. The global transmission

function of this filtering system was modelled with a supergaussian function of the following form,

$$T = \exp\left(- \left(\frac{\lambda - \Lambda_0}{\Delta\lambda} \right)^m \right) \tag{6}$$

The parameters Λ_0, m, and $\Delta\lambda$ where adjusted to obtain the best fit with the experimental spectrum measured after the filtering system. The following values where used: $\Lambda_0 = 11.87$ μm, $m = 80$, and $\Delta\lambda = 10$ μm.

4 Simulation Results

In this section, we present simulation results for three different pump pulse durations: 50 ps, 200 ps, and 460 ps (the measured experimental duration). For the simulations, a Gaussian pulse was used. Quantum noise was added to the initial pulse following the one photon per mode model (see [39] for more details). The numerical models used for each fiber are also presented, including dispersion, nonlinear parameters and losses. A peak power of 6 kW was chosen for the three pump pulses to get the best match with experimental results. For this type of simulation, we typically use a lower peak power than the experimental peak power, which is around 18 kW in this case. This is due to the fact that the simulation model considers perfectly polarized and single-mode propagation. In experimental conditions, random polarization and multi-mode behavior is generally detrimental to spectral broadening mechanisms, hence the need for more peak power than in simulations. Simulations were carried out for the three pump pulse durations in the SMF-28 fiber and the ZBLAN fiber. As expected from the theory of SC generation with quasi-CW pulses, we show that the same mechanisms occur for the three different pump pulse durations, and that the experimental SC bandwidths at the output of the ZBLAN and chalcogenide fibers can be achieved with pump pulses as short as 50 ps. The SSFM algorithm requires high longitudinal precision in the chalcogenide fiber because of high nonlinearity ($\gamma_0 = 720$ km^{-1}W^{-1}). As a result, simulations for 200 ps and 460 ps pump pulses, which require at least $\texttt{Nt} = 2^{21}$ sample points, would require unrealistic computing times. Therefore, simulations in the chalcogenide fiber were only carried out with the intermediate ZBLAN results from the 50 ps pump pulse.

4.1 Single-mode silica fiber

The simulation results for 20 cm of propagation in the single-mode silica fiber (SMF-28) are shown in figure 5 for a 460 ps pulse. The pulse shape remains virtually unchanged throughout this fiber segment. The only notable feature is the apparition of weak MI sidebands in the spectrum around 1.51 and 1.59 μm. They can be seen appearing on either side of the pump in the spectral evolution (figure 5 on the right). Their specific frequencies relative to the pump (Ω_{MI}) are given by the phase-matching condition that reads as $\beta_2\Omega_{\text{MI}}^2 + \frac{\beta_4}{12}\Omega_{\text{MI}}^4 + 2\gamma P_0 = 0$, Where P_0 is the peak power, γ is the nonlinear parameter, β_2 is the GVD parameter, and β_4 is the fourth-order dispersion parameter. A more detailed view is shown in figure 7. It is worth noting, however, that our simulations show this first fiber segment has little to no effect on the overall SC evolution in the ZBLAN and chalcogenide fibers.

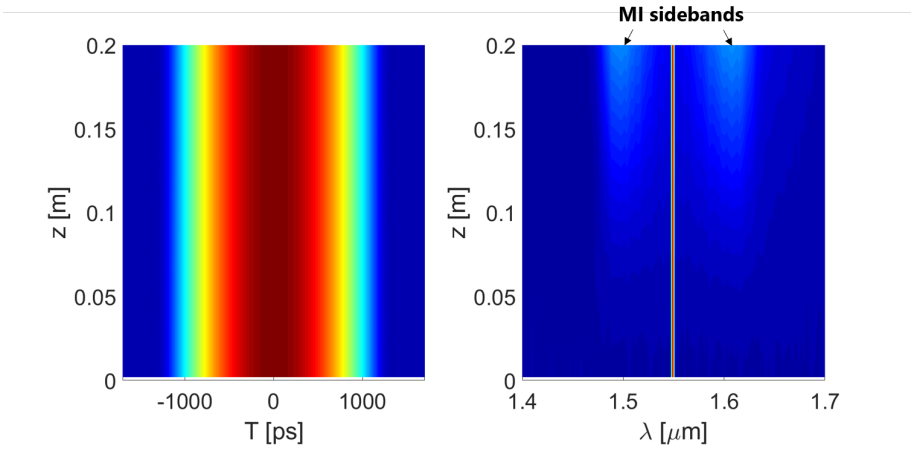

Figure 5: Temporal and spectral evolution in the SMF-28 fiber for a 460 ps pulse. The spectral and temporal evolution in all figures are represented with color maps of relative intensity with a 40 dB range from blue to red.

4.2 ZBLAN Fiber

The simulated spectral and temporal evolution in both the SMF-28 and the ZBLAN fibers are shown in figure 6. On the right, the final spectrum after 25 m of propagation is compared to the experimental spectrum. The agreement is particularly excellent. This is due to the fact that the total bandwidth and soliton RIFS is only limited by the transmission window of the fiber (see figure **??**) in the mid-infrared, which ends between 4 and 4.5 μm. The break-up of the pulse into a train of solitons can be seen from 2 m in Fig. 6(b). Beyond this point, the continuous Raman-induced self-frequency shift of the solitons is clearly seen in the spectral evolution and in the temporal evolution as they gradually separate from the main pulse due to their dispersion increasing with the SSFS. Events of soliton collision can also be observed in the spectral evolution. They manifest themselves as sharp increases in the spectrum bandwidth on the long-wavelength side (e.g. around 16 m in the 50 ps spectral evolution). Dispersive waves can be seen rapidly drifting away from the main pulse in the time evolution. In terms of bandwidth, the simulation provide a nearly perfect match with the experimental spectrum (within 0.05 μm at the -20 dB points).

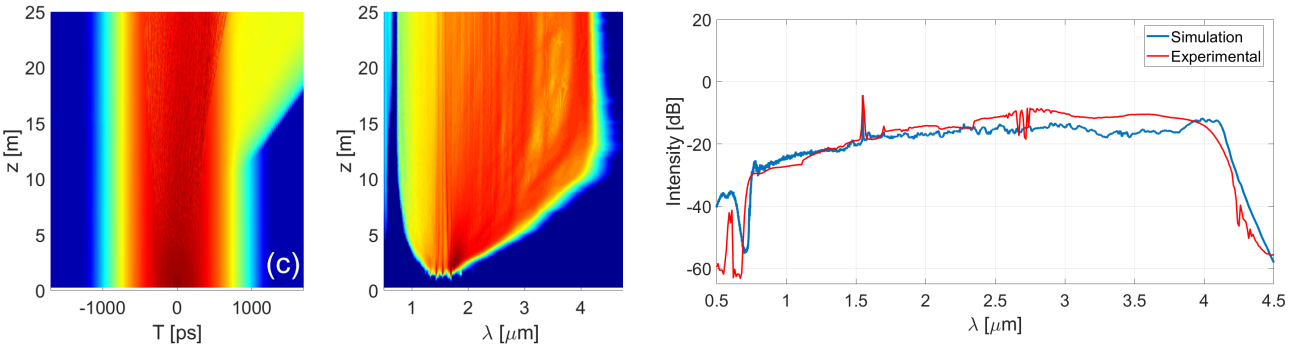

Figure 6: Spectral and time-domain evolution for the 460 ps pump pulse with the output experimental and numerical spectra on the right.

To gain insight on the processes initiating SC generation in the ZBLAN fiber, we show in figure 7 the

details of the first 50 cm of spectral evolution. The strongest sidebands correspond to the MI-enabled Stokes and anti-Stokes Raman sidebands around 1.42 and 1.70 μm. Around 1.51 and 1.59 μm are the residual MI sidebands from the SMF-28 fiber. Very weak MI ZBLAN sidebands are visible around 1.39 and 1.755 μm. Each of the wavelength pairs given here and identified on the plot were calculated theoretically. The MI wavelengths can be derived from the same equation as for the SMF-28 fiber, and the Raman wavelengths correspond to the peak of the ZBLAN Raman gain (figure 3), at 17.4 THz. As discussed in the theory section, this gradual amplification of noise breaks up the pulse into a train of femtosecond pulses, as seen in figure **??**.

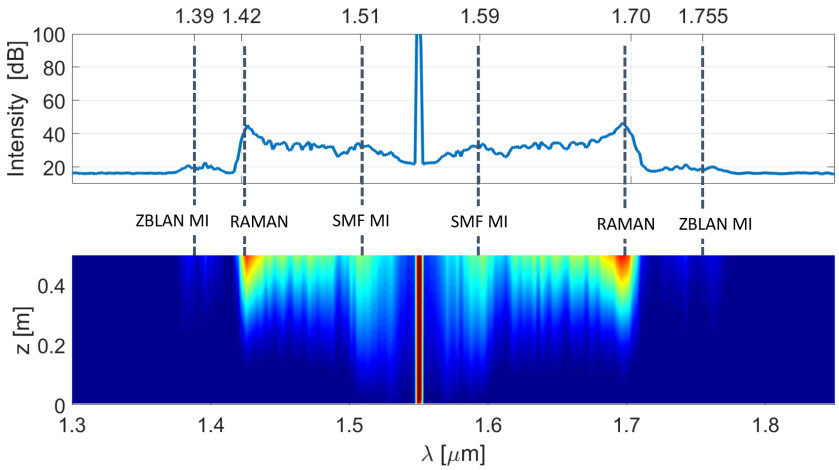

Figure 7: Initial spectral evolution in the ZBLAN fiber. The wavelengths marked with the dotted lines correspond to the theoretical MI and Raman wavelengths calculated with equation **??** and the Raman gain peak at 17.4 THz respectively.

From theory and simulation, we confirm that the time and spectral domain evolution of the 460 ps pulse is very well approximated by the 50 ps pulse. Therefore, from now on, simulations are carried out only with the 50 ps pump pulse to save computing time. Figure 8 shows the filtered simulated spectrum compared with the experimental filtered spectrum using 50-ps input pulse. This is the spectrum injected in the chalcogenide fiber. The dynamics of the experimental spectrum are related to the measurement technique and not a consequence of actual SC dynamics.

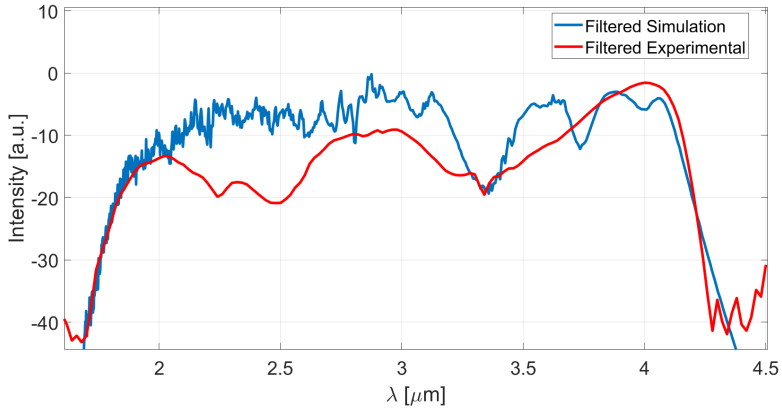

Figure 8: Filtered spectrum injected in the chalcogenide fiber.

4.3 Chalcogenide Fiber

The simulation result for the first 2 cm of propagation in the chalcogenide fiber are shown in Fig. 9. The injected spectrum from the filtered ZBLAN output lies entirely in the normal dispersion regime of the chalcogenide fiber which has its ZDW at 4.838 μm (marked by the dotted line). The initial spectral evolution shows that, from the train of thousands of pulses injected in the chalcogenide fiber, a fraction of them have a small enough width T_0 to drift through the zero-dispersion via RIFS (see equation **??**). The pulses crossing the ZDW evolve back into solitons and create an initial low-intensity continuum on the long-wavelength side through RIFS.

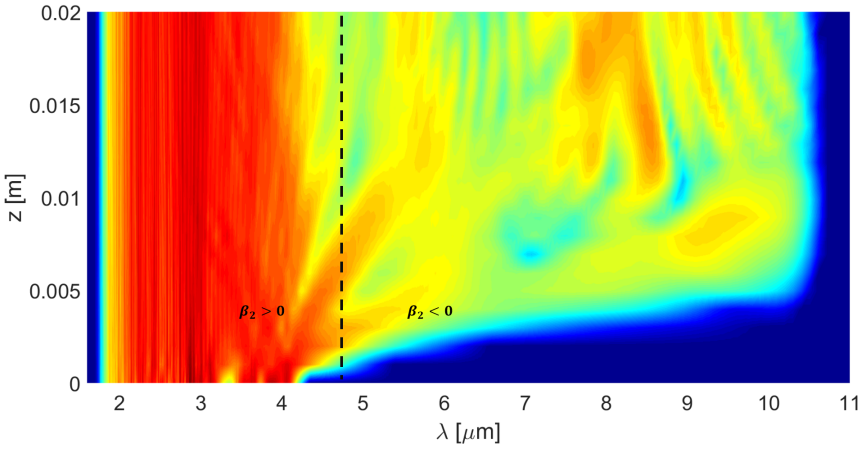

Figure 9: Initial spectral evolution in the chalcogenide fiber.

The spectral evolution over the full 9 m of chalcogenide fiber is shown in figure 10. The top of the figure shows the final output spectrum compared to the experimental spectrum. In terms of spectral bandwidth, our numerical result matches nearly perfectly with the experimental measurement (the -20 dB points of the simulation are within 0.04 μm of the experimental -20 dB points). As for the ZBLAN fiber, spectral broadening in the chalcogenide fiber is only limited by its transmission window.

The spectral evolution of figure 10 shows interesting SC dynamics. From 0 to 5 m, most of the

energy remains in the normal dispersion regime ($\beta_2 > 0$). Energy rapidly accumulates at the limit of the transmission window (around 9.5 μm) from the pulses that initially crossed the ZDW. These solitons tend to accumulate around this wavelength as their SSFS is stopped by the upper limit of the transmission window. The effect of the absorption peak at around 4.6 μm (see figure **??**) can be clearly seen on the low-energy continuum. From the beginning, the main train of pulses can be seen drifting (though SSFS) towards the ZDW. After 5 m most of the pulses remain *trapped* by the ZDW barrier and stop their frequency drift. From 5 m onwards, a fraction of the pulses cross the ZDW barrier and start evolving as solitons on the anomalous dispersion side ($\beta_2 < 0$). This gradually adds energy to the initial low-energy continuum via the RIFS of the solitons. The spectrum evolves towards *thermalization*, where energy is equally distributed throughout the transmission bandwidth. The output is therefore a relatively flat spectrum from 2 to 9.7 μm.

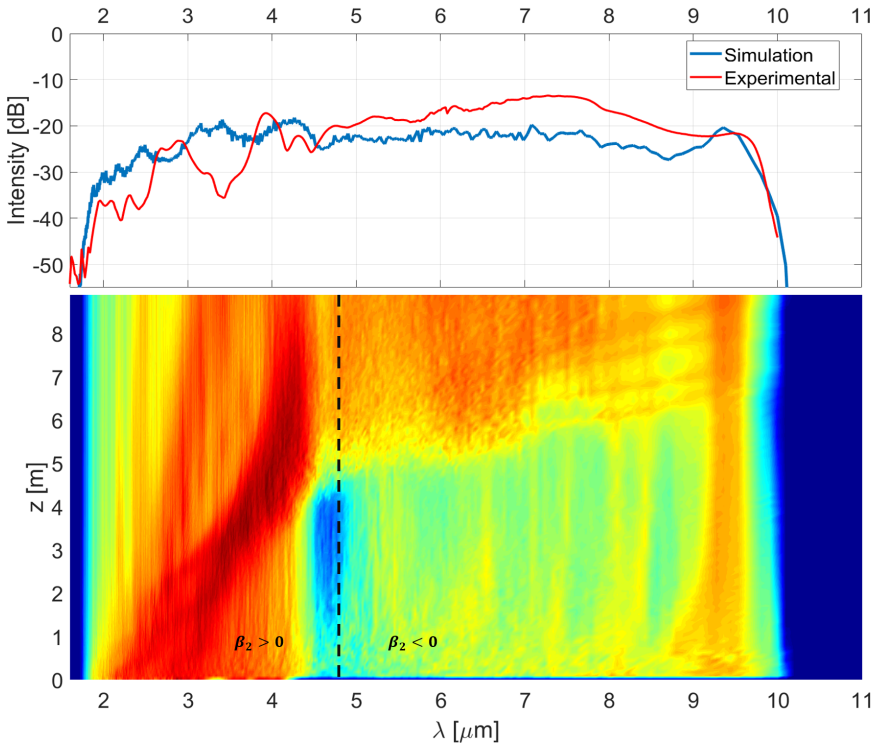

Figure 10: Full spectral evolution in the chalcogenide fiber with final output spectrum.

5 Conclusion and Recommendations

In this work, we have developed a broadband all-fiber supercontinuum source spanning from 2 to 10 μm with 16 mW output power. This was achieved using cascaded ZBLAN-chalcogenide optical fibers directly pumped by a 1550 nm picosecond Erbium-doped fiber laser without any fiber amplifier. We have further carried numerical simulations for broadband mid-infrared SC generation in a cascaded fiber system. Our simulations were consistent with the theory of quasi-CW SC generation. We show that noise amplification through MI and Raman gain leads to the break-up of the pulse envelope into a chaotic train of solitons which broadens the spectrum through Raman-induced self-frequency shift and dispersive waves. In terms of bandwidth, our numerical results are nearly identical to the experimentally measured spectra, both at the output of the ZBLAN fiber (within 0.05 μm at -20 dB points) and the chalcogenide fiber (within 0.04 μm at -20 dB points). The final output spectrum is a flat broadband spectrum covering the mid-IR from 2 to 10 μm. Further broadening is only limited by the transmission window of the chalcogenide fiber. Our main recommendation consists of using a chalcogenide microstructured fiber with a smaller core diameter as the third fiber of the cascaded system [47]. This would shift its zero-dispersion wavelength towards shorter wavelengths and allow to fill the desired window (from 2 to 10 μm) with a few tens of centimeters of fiber only. Our second recommendation consists of exploring different options for the infrared filtering system and to avoid free-space optics. The free-space optics and the re-coupling to the chalcogenide fiber induce considerable losses in the system. An all-fiber filtering system, for example, could provide more robustness and less loss. Finally, we also recommend exploring telluride-based fibers as a fourth fiber to add to the system. This would potentially allow to further broaden the spectrum and reach wavelengths beyond 10 μm [46]. Nevertheless, we believe that, despite the mentioned weaknesses, current mid-infrared supercontinuum all-fiber sources can find strong potential applications and it may represent a landmark to foster the improvement of such broadband sources in other different photonic platforms.

6 Funding informations

This project has received funding from the Agence Nationale de la Recherche (ANR) (ANR-15-IDEX-0003, ANR-17-EURE-0002) and the European Union H2020 programme MSCA-ITN-SUPUVIR under grant agreement 722380.

7 Supplementary informations

In this section, we present simulation results for the same cascaded fiber system, but with a different chalcogenide fiber to study the effect of the zero-dispersion wavelength. The chosen fiber was presented by Saghaei *et al.* [47] in 2015 as part of an experimental study on mid-infrared SC generation. It is microstructured with the same air-hole pattern as the one used experimentally. Figure 11 shows a diagram of its cross-section. It is made of As_2Se_3 glass, which has similar nonlinear properties to $As_{38}Se_{62}$ glass. The main difference is its lower ZDW, which is at 3.81 μm. This is due to the different dimensions of its air-hole structure: it has a core diameter of 7 μm, a pitch of 5 μm, and an air-hole diameter of 3 μm.

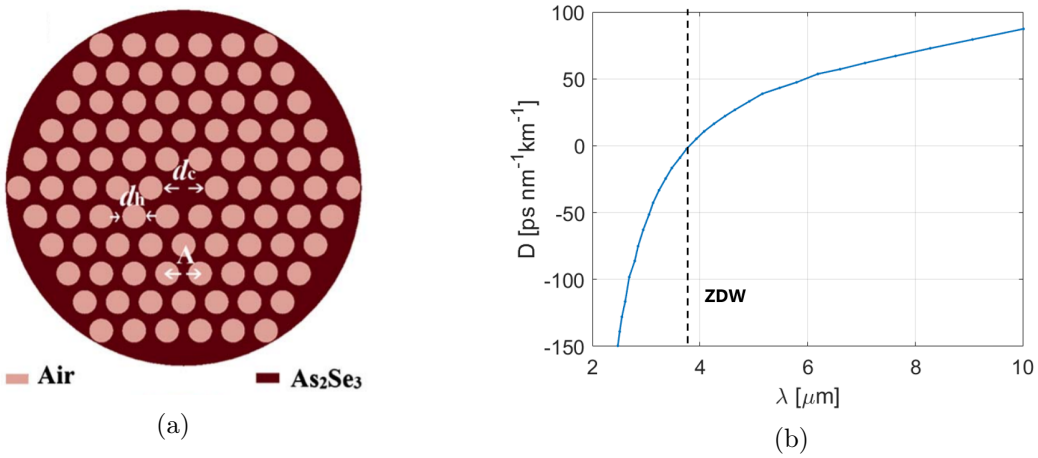

(a) (b)

Figure 11: (a) Cross-section of the alternative chalcogenide fiber (adapted from [47]). (b) Dispersion curve.

Figure 12 shows the spectral evolution over 1 cm of this alternative chalcogenide fiber. This short propagation distance allowed to carry out the simulation with the filtered ZBLAN spectrum from a 460 ps pump pulse. With the ZDW at 3.81 μm, a fraction of the filtered ZBLAN output spectrum is injected directly in the anomalous dispersion regime of this fiber (on the right of the dotted line in figure 12). This allows a great number of solitons to form directly without having to cross the ZDW barrier. Through RIFS, the solitons rapidly fill the transmission window with a relatively high-energy continuum. Therefore, by shifting the ZDW to 3.81 μm with this alternative chalcogenide fiber, our simulations show that an almost flat SC spanning the 2-10 μm window can be generated with only 1 cm of fiber.

The study of broadening dynamics in this fiber shows that, over the first centimeters of propagation, energy injected in the normal dispersion regime tends to stay concentrated on that side of the ZDW, and energy injected in the anomalous dispersion regime rapidly spreads to fill the transmission window. Therefore, we can postulate that shifting the ZDW further towards short wavelengths (with an even smaller core diameter) would help achieve an even flatter SC with only a few centimeters of fiber. This would reduce cost and the overall losses in the cascaded system.

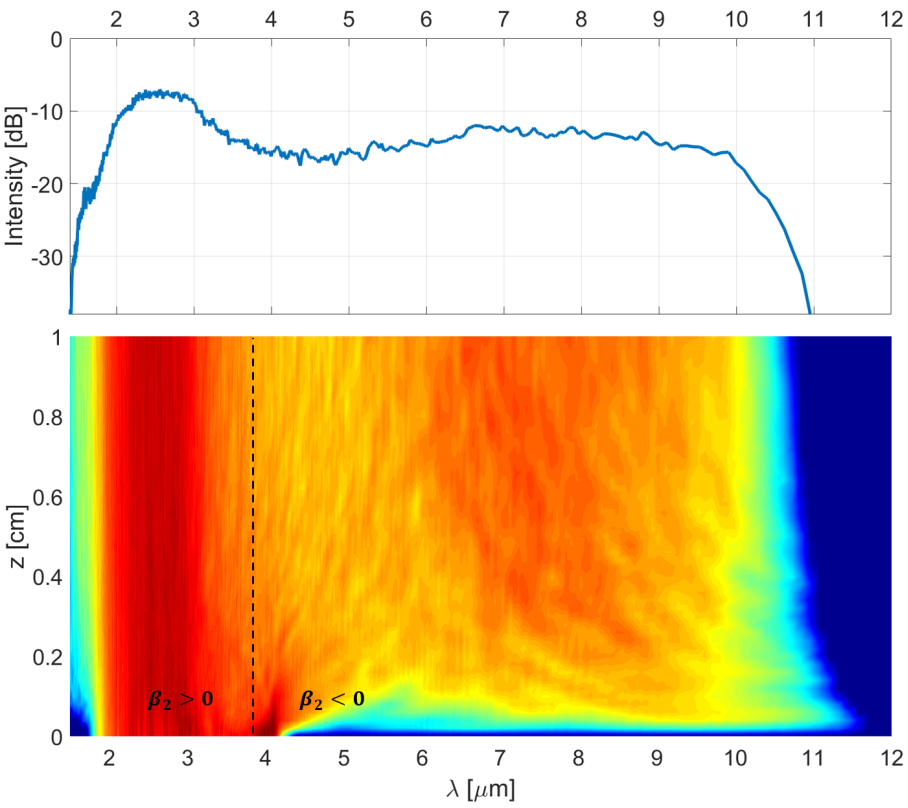

Figure 12: Spectral evolution in the 7 μm-core chalcogenide fiber.

References

[1] R. R. Alfano, The Supercontinuum Laser Source: The Ultimate White Light (Springer, New York, 2016).

[2] Dudley, J. M., Taylor, J. R. (Eds.). (2010). *Supercontinuum generation in optical fibers*. Cambridge University Press.

[3] C. R. Petersen, U. Møller, I. Kubat, B. Zhou, S. Dupont, J. Ramsay, T. Benson, S. Sujecki, N. A. -Moneim, Z. Tang, D. Furniss, A. Seddon, and O. Bang, "Mid-infrared supercontinuum covering the 1.4–13.3 μm molecular fingerprint region using ultra-high NA chalcogenide step-index fibre", Nat. Photon. 8, 830-834 (2014).

[4] Yu, Y., Zhang, B., Gai, X., Zhai, C., Qi, S., Guo, W., Yang, Z., Wang, R., Choi, D., et al., "1.8-10 μm mid-infrared supercontinuum generated in a step-index chalcogenide fiber using low peak pump power," Optics Letters 40 (6), 1081–1084 (2015).

[5] T. Cheng, K. Nagasaka, T. H. Tuan, X. Xue, M. Matsumoto, H. Tezuka, T. Suzuki, and Y. Ohishi, "Mid-infrared supercontinuum generation spanning 2.0 to 15.1 μm in a chalcogenide step-index fiber", Opt. Lett. 41 (9), 2117-2120 (2016).

[6] Uffe Møller, Yi Yu, Irnis Kubat, Christian R. Petersen, Xin Gai, Laurent Brilland, David Méchin, Celine Caillaud, Johann Troles, Barry Luther-Davies, and Ole Bang, "Multi-milliwatt mid-infrared supercontinuum generation in a suspended core chalcogenide fiber," Opt. Express 23, 3282-3291 (2015).

[7] A. Lemière, F. Désévédavy, P. Mathey, P. Froidevaux, G. Gadret, J.-C. Jules, C. Aquilina, B. Kibler, P. Béjot, F. Billard, O. Faucher, and F. Smektala, "Mid-Infrared supercontinuum generation from 2 to 14 μm in arsenic- and antimony-free chalcogenide glass fibers", J. Opt. Soc. Am. B 36, A183-A192 (2019).

[8] C. R. Petersen, R. D. Engelsholm, C. Markos, L. Brilland, C. Caillaud, J. Troles, and O. bang, "Increased mid-infrared supercontinuum bandwidth and average power by tapering large-mode-area chalcogenide photonic crystal fibers", Opt. Express 25 (13), 15336-15347 (2017).

[9] Dai, Shixun and Wang, Yingying and Peng, Xuefeng and Zhang, Peiqing and Wang, Xunsi and Xu, Yinsheng, "A Review of Mid-Infrared Supercontinuum Generation in Chalcogenide Glass Fibers", Applied Sciences 8 (5), 707 (2018).

[10] A. N. Ghosh, M. Klimczak, R. Buczynski, J. M. Dudley, and T. Sylvestre, "Supercontinuum generation in heavy-metal oxide glass based suspended-core photonic crystal fibers", J. Opt. Soc. Am. B 35, 2311-2316 (2018).

[11] F. Belli, A. Abdolvand, W. Chang, J.C. Travers, and P. St. J. Russell, "Vacuum-ultraviolet to infrared supercontinuum in hydrogen-filled photonic crystal fiber", Optica 2 (4), 292-300 (2015).

[12] N. M. Israelsen, C. R. Petersen, A. Barh, D. Jain, M. Jensen, G. Hannesschläger, P. T. -Lichtenberg, C. Pedersen, A. Podoleanu, and Ole Bang, "Real-time high-resolution mid-infrared optical coherence tomography", Light: Science and Applications, 8, 11 (2019).

[13] I. Zorin, R. Su, A. Prylepa, J. Kilgus, M. Brandstetter, and B. Heise, "Mid-infrared Fourier-domain optical coherence tomography with a pyroelectric linear array", Opt. Express 26, 33428-33439 (2018).

[14] J. Hult, R. S. Watt, and C. F. Kaminski, "High bandwidth absorption spectroscopy with a dispersed supercontinuum source", Opt. Express 15 (18), 11385-11395 (2007).

[15] C. Amiot, A. Aalto, P. Ryczkowski, J. Toivonen, and G. Genty, "Cavity enhanced absorption spectroscopy in the mid-infrared using a supercontinuum source", Appl. Phys. Lett. 111 (6), 061103 (2017).

[16] C. R. Petersen, P. M. Moselund, L. Huot, L. Hooper, and O. Bang, "Towards a table-top synchrotron based on supercontinuum generation", Infrared Physics and Technology 91, 182-186 (2018).

[17] A. B. Seddon, "Biomedical Applications in Probing Deep Tissue Using Mid-Infrared Supercontinuum Optical Biopsy" in book "Deep Imaging in tissue and biomedical Media" by L. Shi and R. R. Alfano (Pan Stanford Publishing, Singapore, pp 231-294 (2016).

[18] C. R. Petersen, N. Prtljaga, M. Farries, J. Ward, B. Napier, G. R. Lloyd, J. Nallala, N. Stone, and O. Bang, "Mid-infrared multispectral tissue imaging using a chalcogenide fiber supercontinuum source", Opt. Lett. 43(5), 999-1002 (2018).

[19] F. Désévédavy, G. Gadret, J. -C. Jules, B. Kibler, and F. Smektala, "Supercontinuum Generation in Tellurite Optical Fibers", Technological Advances in Tellurite Glasses, Springer Ser. Mater. Sci., vol 254, Springer (2017).

[20] P. Lucas, Z. Yang, M. K. Fah, T. Luo, S. Jiang, C. Boussard-Pledel, M.-L. Anne, and B. Bureau, "Telluride glasses for far infrared photonic applications," Opt. Mater. Express 3, 1049-1058 (2013).

[21] Z. Zhao, B. Wu, X. Wang, Z. Pan, Z. Liu, P. Zhang, X. Shen, Q. Nie, S. Dai, and R. Wang, "Mid-infrared supercontinuum covering 2.0–16 μm in a low-loss telluride single-mode fiber", Laser Photonics Rev. 11, No. 2 (2017).

[22] C. Xia, M. Kumar, O. P. Kulkarni, M. N. Islam, F. L. Terry, M. J. Freeman, M. Poulain, and G. Mazé, "Mid-infrared supercontinuum generation to 4.5 μm in ZBLAN fluoride fibers by nanosecond diode pumping", Opt. Lett. 31 (17), 2553-2555 (2006).

[23] M. Michalska, P. Hlubina, and J. Swiderski, "Mid-infrared Supercontinuum Generation to 4.7 μm in a ZBLAN Fiber Pumped by an Optical Parametric Generator", IEEE Photon. J. 9 (2), 3200207 (2017).

[24] C. Agger, C. Petersen, S. Dupont, H. Steffensen, J. K. Lyngsø, C. L. Thomsen, J. Thøgersen, S. R. Keiding, and O. Bang, "Supercontinuum generation in ZBLAN fibers—detailed comparison between measurement and simulation", J. Opt. Soc. Am. B 29 (4), 635-645 (2012).

[25] Hagen, C.L.,Walewski, J.W. and Sanders, S.T., "Generation of a continuum extending to the mid-infrared by pumping ZBLAN fiber with an ultrafast 1550 nm source", IEEE Phot. Tech. Lett. 18, 91–93, (2006).

[26] Xia, C., Kumar, M., Cheng, M.Y., Hegde, R.S., Islam, M.N., Galvanauskas, A., Winful, H.C. and Terry Jr, F.I. "Power scalable mid-infrared supercontinuum generation in ZBLAN fluoride fibers with up to 1.3 watts time-averaged power", Opt. Exp. 15, 865–871 (2007).

[27] Darren D. Hudson, Sergei Antipov, Lizhu Li, Imtiaz Alamgir, Tomonori Hu, Mohammed El Amraoui, Younes Messaddeq, Martin Rochette, Stuart D. Jackson, and Alexander Fuerbach, "Toward all-fiber supercontinuum spanning the mid-infrared," Optica 4, 1163-1166 (2017).

[28] F. Theberge, N. Berube, S. Poulain, S. Cozic, S. Chatigny, L.-R. Robichaud, L.-P. Pleau, M. Bernier, and R. Vallee, "Infrared supercontinuum generated in concatenated InF3 and As2Se3 fibers", Opt. Express 26 (11), 13952-13960 (2018).

[29] R. A. Martinez, G. Plant, K. Guo, B. Janiszewski, M. J. Freeman, R. L. Maynard, M. N. Islam, F. L. Terry, O. Alvarez, F. Chenard, R. Bedford, R. Gibson, and A. I. Ifarraguerri, "Mid-infrared supercontinuum generation from 1.6 to >11 μm using concatenated step-index fluoride and chalcogenide fibers", Opt. Lett. 43 (2), 296-299 (2018).

[30] R. A. Martinez, K. Guo, T. Zhai, F. L. Terry, L. E. Pierce, M. N. Islam, R. Gibson, J. M. Reed, R. G. Bedford, L. Maksymiuk, M. J. Freeman, B. A. Gorin, N. P. Christian, and A. I. Ifarraguerri, "Active Mid-Wave to Long-Wave Supercontinuum FTIR Sensor for Standoff Chemical Detection," J. Lightwave Technol. 37, 3626-3636 (2019)

[31] I. Kubat, C. R. Petersen, U. Visbech Møller, A. Seddon, T. Benson, L. Brilland, D. Méchin, P. M. Moselund, and O. Bang, "Thulium pumped mid-infrared 0.9–9 μm supercontinuum generation in concatenated fluoride and chalcogenide glass fibers," Opt. Express 22, 3959-3967 (2014).

[32] Christian Rosenberg Petersen, Peter M. Moselund, Christian Petersen, Uffe Møller, and Ole Bang, "Spectral-temporal composition matters when cascading supercontinua into the mid-infrared," Opt. Express 24, 749-758 (2016).

[33] C. R. Petersen, P. M. Moselund, Ch. Petersen, U. Møller, O. Bang, "Mid-IR supercontinuum generation beyond 7μm using a silica-fluoride-chalcogenide fiber cascade," Proc. SPIE 9703, Optical Biopsy XIV: Toward Real-Time Spectroscopic Imaging and Diagnosis, 97030A (2016);

[34] http://norblis.com/

[35] Jinmei Yao, Bin Zhang Ke Yin, and Jing HouJinmei, "The 2-μm to 6-μm mid-infrared supercontinuum generation in cascaded ZBLAN and As2Se3 step-index fibers," Chinese Phys. B 28 084209 (2019).

[36] Dudley, J. M., Genty, G., Coen, S. (2006). Supercontinuum generation in photonic crystal fiber. *Reviews of modern physics*, 78(4), 1135.

[37] Agrawal, G. P. (2000). *Nonlinear fiber optics*. In Nonlinear Science at the Dawn of the 21st Century. Springer, Berlin, Heidelberg.

[38] Sánchez, A. D., Fierens, P. I., Hernandez, S. M., Bonetti, J., Brambilla, G., Grosz, D. F. (2018). Anti-Stokes Raman gain enabled by modulation instability in mid-IR waveguides. *JOSA B*, 35(11), 2828-2832.

[39] Genier, E., Bowen, P., Sylvestre, T., Dudley, J. M., Moselund, P., Bang, O. (2019). Amplitude noise and coherence degradation of femtosecond supercontinuum generation in all-normal-dispersion fibers. *JOSA B*, 36(2), A161-A167.

[40] ZFG Singlemode. (n.d.). https://leverrefluore.com/products/passive-fibers/zfg-singlemode/

[41] Fluoride fiber technology. (n.d.). Retrieved from https://www.fiberlabs.com/glossary/technology/

[42] Hudson, D. D., Antipov, S., Li, L., Alamgir, I., Hu, T., El Amraoui, M., Fuerbach, A. ,"Toward all-fiber supercontinuum spanning the mid-infrared," *Optica*, 4(10), 1163-1166 (2017).

[43] B. Kibler, J. M. Dudley, S. Coen, "Supercontinuum generation and nonlinear pulse propagation in photonic crystal fiber: influence of the frequency-dependent effective mode area," *Applied Physics* B, 81(2-3), 337-342 (2005).

[44] Sinkin, O. V., Holzlohner, R., Zweck, J., Menyuk, C. R. (2003). Optimization of the split-step Fourier method in modeling optical-fiber communications systems. *Journal of lightwave technology*, 21(1), 61-68.

[45] Q. Coulombier, L. Brilland, P. Houizot, T. Chartier, T. N. N'Guyen, F. Smektala, G. Renversez, A. Monteville, D. Mechin, T. Pain, H. Orain, J.-C. Sangleboeuf, and J. Troles, "Casting method for producing low-loss chalcogenide microstructured optical fibers," Opt. Express 18, 9107-9112 (2010).

[46] Cui, S., Boussard-Plédel, C., Troles, J., Bureau, B. (2016). Telluride glass single mode fiber for mid and far infrared filtering. *Optical Materials Express*, 6(4), 971-978.

[47] Saghaei, H., Ebnali-Heidari, M., Moravvej-Farshi, M. K. (2015). Midinfrared supercontinuum generation via As2Se3 chalcogenide photonic crystal fibers. *Applied optics*, 54(8), 2072-2079.